

Supporting Information

Lipid Anchor Display on Peptoid Nanosheets via Co-Assembly for Multivalent Pathogen Recognition

Jae Hong Kim¹, Elissa M. Grzincic¹, Lisa Yun¹, Ryan K. Spencer², Mark A. Kline¹, Ronald N. Zuckermann^{*1}

¹Molecular Foundry, Lawrence Berkeley National Laboratory, 1 Cyclotron Road, Berkeley CA 94720, United States.

²Department of Chemistry and Department of Chemical Engineering & Materials Science, University of California, Irvine, Irvine, California

*rnzuckermann@lbl.gov

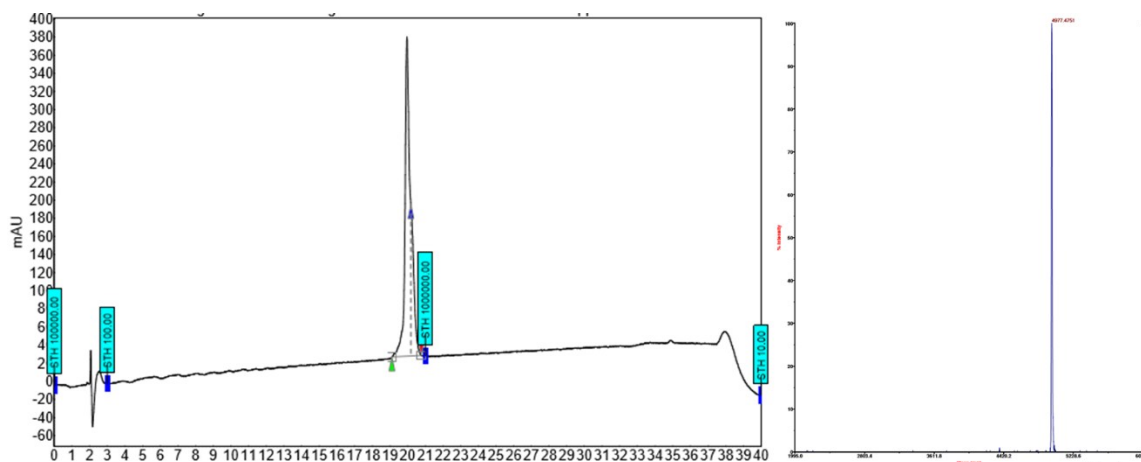
1. MATERIALS.....	2
A1. Chemicals and synthesis of peptoid strands.....	2
A2. Expression of STX 1B and E. coli. Strains.....	4
2. METHODS.....	5
B1. Nanosheet production.....	5
B2. Characterization of nanosheet.....	5
B3. Homogeneous FRET assay.....	6
B4. Inhibition test of E. Coli Growth.....	6
3. SUPPLEMENTARY DATA.....	7
Figure S1. Fluorescent images of B36 nanosheets with fluorophores and Dye-conjugated lipids.	
Figure S2. Langmuir isotherms of B36 in the absence and presence of dye-conjugated lipids (2 , 3 and 4).	
Figure S3. Relative productivity of peptoid nanosheets in the presence of 1 – 4 .	
Figure S4. Stability of lipids in peptoid nanosheets.	
Figure S5. Distance between lipids based on molecular structure and FRET assay.	
Figure S6. Distance between loops and pockets in peptoid nanosheets.	
Figure S7. Molecular structure of B36/ 5 and 6 by MD simulation.	
Figure S8. Molecular structure of STX 1B.	
Figure S9. Fluorescent spectra of B36 and B36/ 6 in the absence and presence of STX 1B.	
Figure S10. Confocal images of B36, B36/ 7 in the absence and presence of <i>E. coli</i> ORN178 and ORN208.	
Figure S11. Effect of lipid concentration to capture <i>E. Coli</i> .	
Figure S12. <i>E. Coli</i> aggregation on the surface of B36/ 7 .	
4. REFERENCES.....	16

1. MATERIALS

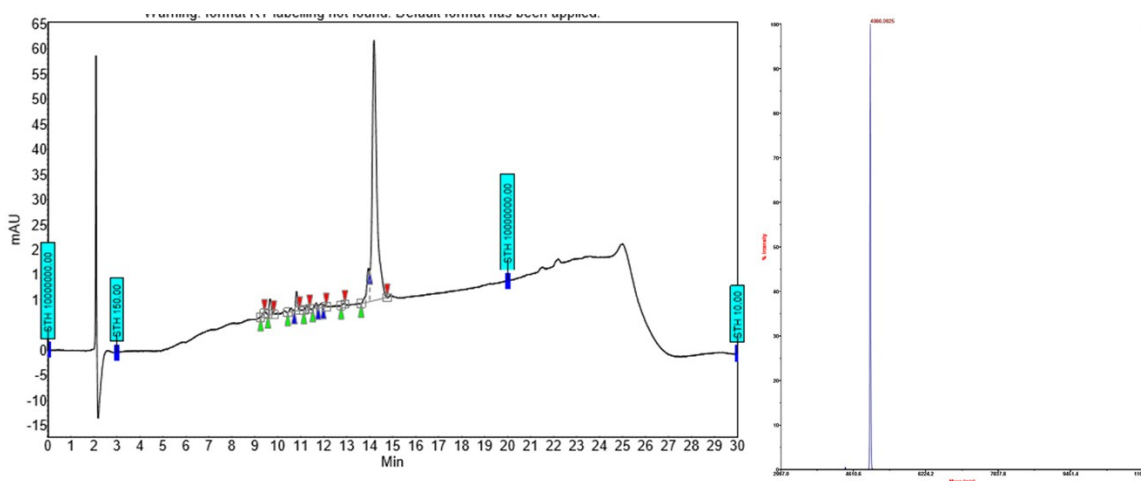
A1. Chemicals and synthesis of peptoids.

All chemicals (e.g., potassium iodide, Alexa Fluor 488- and Alexa Fluor 647-maleimide) and lipids were purchased from Sigma-Aldrich, ThermoFisher Scientific, and Avanti Lipids Polar. Peptoid strands, such as B36 and thiol-functionalized B36 (SH-B36), were synthesized by solid-phase submonomer method according to the literature.¹ Alexa Fluor 488- and Alexa Fluor 647-maleimide were conjugated to SH-B36 for the preparation of dye-conjugated peptoid strands. Briefly, we prepared glass vial containing 2 mg of purified and lyophilized SH-B36 dissolved in 2 mL DMF/Tris HCl buffer (10 mM, pH 7.5) mixture (v/v ~ 1/1). For preventing aggregation of SH-B36, we added 8 mL of 0.5 M tris(2-carboxyethyl)phosphine into the mixture. 1 mg of Alexa Fluor-maleimide was dissolved in 200 μ L of Tris-buffer (10 mM, pH 7.5). Then, Alexa Fluor-containing solution were dropped into the glass vial containing SH-B36. After 5 hours, the reaction mixture was evaporated and washed with acetonitrile using Biotage evaporator. The crude dye-conjugated peptoid strands were purified by reverse phase preparative HPLC. Then, products were characterized by reverse phase analytical HPLC.

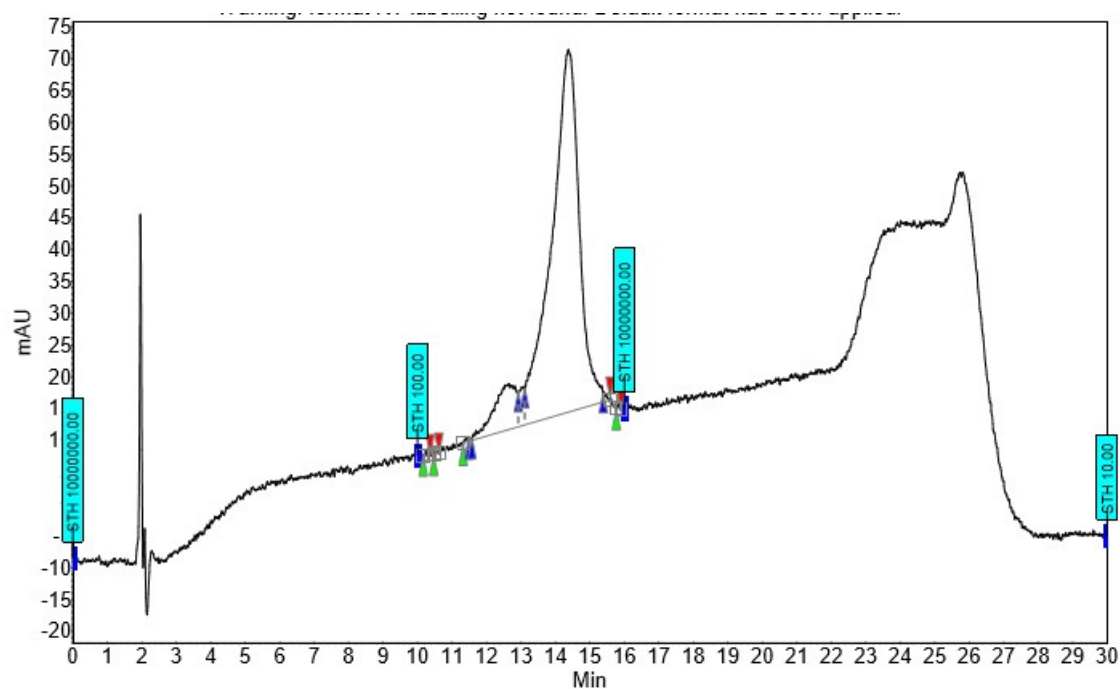
Analytical HPLC spectra and MALDI-TOF spectra of B36:



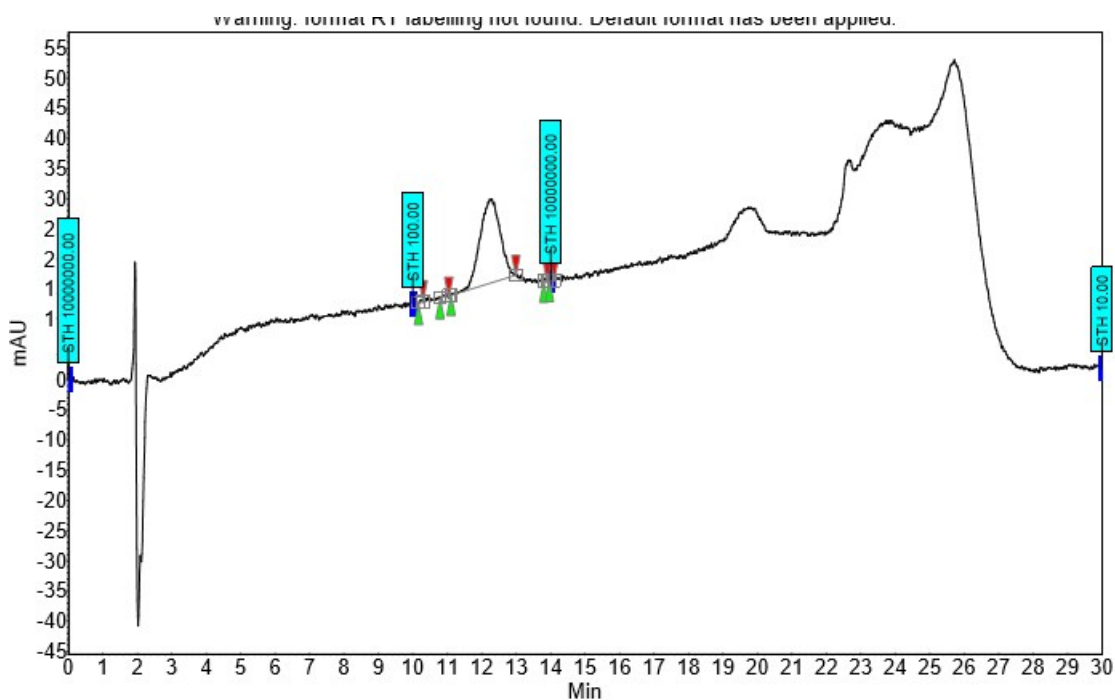
Analytical HPLC spectra and MALDI-TOF spectra of SH-B36:



Analytical HPLC spectra of Alexa Fluor 488-conjugated B36:



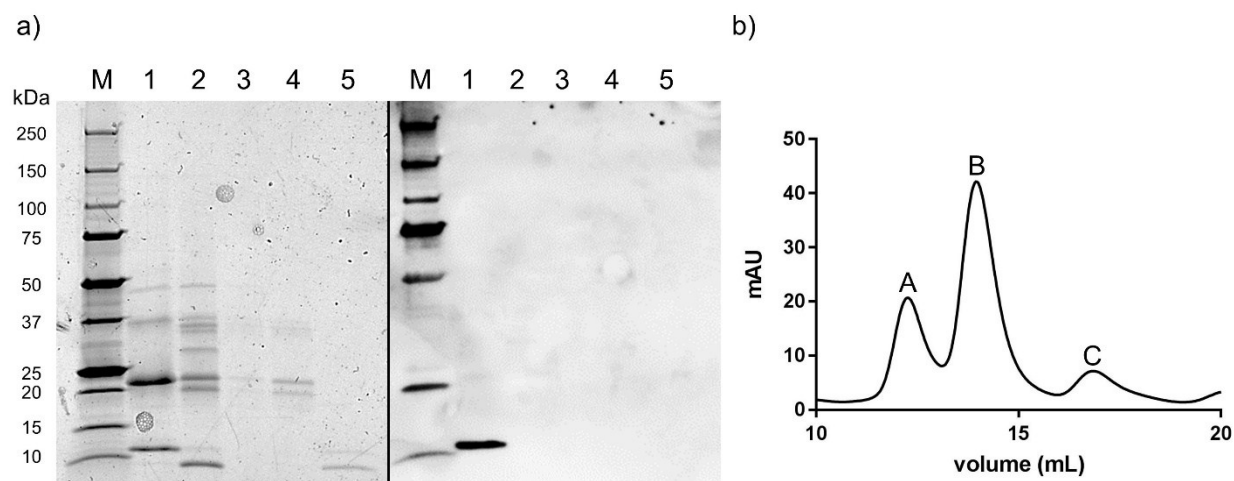
Analytical HPLC spectra of Alexa Fluor 647-conjugated B36:



A2. Expression of STX 1B and *E. coli* Strains

The gene for shiga toxin 1, subunit B (STX 1B) was cloned into a pMAL-c5x vector (New England Biosciences, Ipswich, MA) with a 6X histidine tag, flexible (GGS)₄ linker and tobacco etch virus (TEV) protease cleavage site directly upstream of the gene (no maltose binding protein tag from the vector was included). The plasmid was constructed *via* Gibson Assembly (Gibson Assembly® Master Mix, New England Biosciences, Ipswich, MA) of the linearized vector and the insert as a gene block with 20 base pair overlaps (custom gBlocks® Gene Fragments, Integrated DNA Technologies, Coralville, IA). The plasmid was transformed into chemically competent BL21 (DE3) *E. coli* (New England Biosciences, Ipswich, MA). For expression, 500 mL batches of Luria-Bertani (LB) medium were inoculated to 0.05 OD₆₀₀ and allowed to grow to 0.6-0.8 OD₆₀₀ at 37°C with shaking at 250 rpm. The temperature was then lowered to 30°C and over-expression was induced with 1 mM isopropyl β-D-1-thiogalactopyranoside (IPTG) for 3 hours. Cells were harvested by centrifugation and stored as pellets at -80°C until protein purification. Cells were redispersed in phosphate buffered saline pH 7.4 (PBS; 0.01 M phosphate buffer, 0.0027 M potassium chloride and 0.137 M sodium chloride) with 10 mM imidazole and lysed with an EmulsiFlex C3 homogenizer (Avestin Inc., Ottawa, ON, Canada). Insoluble cell debris was removed by centrifugation and the supernatant was applied to a 1 mL HisTrap™ Excel (GE Healthcare Life Sciences, Marlborough, MA) Ni-NTA column on an ÄKTA FPLC system (GE Healthcare Life Sciences, Marlborough, MA) equilibrated with PBS pH 7.4 with 10 mM imidazole. The column was washed with 40 mM imidazole and bound proteins were eluted with PBS pH 7.4 with 500 mM imidazole. The protein was then dialyzed overnight into PBS pH 7.4 at 4°C, the histidine tag was cleaved with TEV protease overnight at 4°C, and the protein was then purified as a pentamer *via* gel filtration with a Superdex 200 Increase 10/300 GL column (GE Healthcare Life Sciences, Marlborough, MA). Samples were characterized by SDS-PAGE and Western blot (6X-His tag antibody-HRP conjugate; Invitrogen) concentrations were measured by UV-Vis spectroscopy, and samples were stored in PBS pH 7.4 at 4°C.

Alexa Fluor 647 succinimidyl ester (ThermoFisher Scientific, Waltham, MA) was conjugated to solvent-exposed lysine residues of STX 1B. The protein solution was made basic with 1 M sodium bicarbonate (pH 9) and dye was dissolved in dry DMSO. 10 molar equivalents of the dye (relative to pentamer concentration) was added to protein solution while stirring vigorously and reaction was allowed to proceed for 1 hour. The reaction was quenched with 0.2 M tris(hydroxymethyl)aminomethane hydrochloride pH 7.5 and the protein was cleaned by a second round of gel filtration into PBS pH 7.4.



Characterization of expressed STX 1B. (a) SDS-PAGE (left panel) and Western blot with 6X His tag antibody (right panel) of STX 1B purification steps. M = molecular weight markers, 1 = elutant from Ni-NTA column, 2 = after cleavage of tag with TEV protease, 3-5 = fractions corresponding to peaks A-C from gel filtration. (b) Absorbance versus mobile fraction volume of STX 1B sample *via* gel filtration after tag removal.

E. coli ORN178 and ORN208 were kindly provided by the Paul Orndorff lab.² Both strains were transformed with the plasmid pC007 – pRFP which carries the gene for constitutive expression of red fluorescent protein and was a gift from Feng Zhang (Addgene plasmid #79156).³

2. METHODS

B1. Nanosheet formation

The folding of peptoids and lipids into nanosheets was performed by the vial rocking method as previously described.⁴ Briefly, we prepared glass vials containing 500 μ L of 20 μ M peptoid in 10 mM Tris HCl buffer (pH 8.0). Desired concentrations of lipids were added into the nanosheet-forming solution when lipids were incorporated into peptoid nanosheets. The prepared vials were tilted from vertical to horizontal with 10 sec waiting time for up to 250 cycles.

B2. Characterization of peptoid nanosheets

By using Olympus IX81 inverted microscope with fluorescence illumination and Zeiss 710 laser scanning confocal microscope, we observed fluorescent peptoid nanosheets and binding of Alexa Fluor 647-conjugated STX 1B and fluorescent *E. coli* on the peptoid nanosheets.

For the thickness measurement by AFM, nanosheets were dialyzed against nanopure H₂O overnight using 100 kD Float-A-Lyzer dialysis kits. The dialyzed nanosheet solutions were transferred to the surface of freshly cleaved mica. After drying solution, we obtained AFM images and measured thickness using Asylum MFP-3D AFM. The thickness measurements were acquired from the average of three AFM images.

For obtaining XRD spectra, nanosheets were washed and concentrated as reported.⁵ The concentrated nanosheets were deposited on a kapton grid, then XRD spectra were collected at the Advanced Light Source at Lawrence Berkeley National Laboratory.

The fluorescence quenching experiments were performed by the addition of potassium iodide (KI). We prepared 200 μL of 20 μM peptoid nanosheet solution (i.e., Alexa Fluor 488-B36, B36/NR, and B36/1), 80 μL nanopure H_2O and 100 μL of KI at a desired concentration. Then, we measured the fluorescence intensity of the mixture using a fluorescent plate reader (Biotek Synergy H1). The excitation wavelength is 480 nm for Alexa Fluor 488-B36 and 550 nm for B36/NR, and B36/1.

B3. Homogeneous FRET assay

We prepared Alexa Fluor 488-conjugated peptoid nanosheets with different concentration of **6**. 100 μL of the nanosheet solution was mixed with 100 μL of Alexa Fluor 647-conjugated STX 1B at a desired concentration in a 96-well plate. Using a fluorescent plate reader (Biotek Synergy H1), the fluorescence intensities of the samples at 520 and 645 nm were measured under the excitation wavelength at 480 nm. The FRET ratios were calculated by $I_{675\text{ nm}}/I_{520\text{ nm}}$. According to the literature,⁶ we estimated the apparent binding constant (K_D) using Hill's equation by Origin 8.0.

B4. Inhibition of *E. Coli* growth

E. coli ORN178 cells were grown in LB medium overnight at 37°C with shaking. Cells were added to an OD_{600} of 0.05 into 750 μL of nanosheet solution (either Tris buffer control, B36 or B36/20 μM **7**) in a sterile 24-well plate and incubated at 37°C and 250 rpm shaking for 4 hours. During this time, the cells were without growth medium to allow for complete mixing with nanosheets without significant growth. After 4 hours, 250 μL of 4x concentrated LB medium was added to each well to allow growth for another 6 hours. At each hour, an aliquot was removed from each sample into a sterile 96-well plate for OD_{600} measurements, then replaced into the sample well. Controls for nanosheet scattering (without cells) and pathlength corrections were performed as well.

3. SUPPLEMENTARY DATA

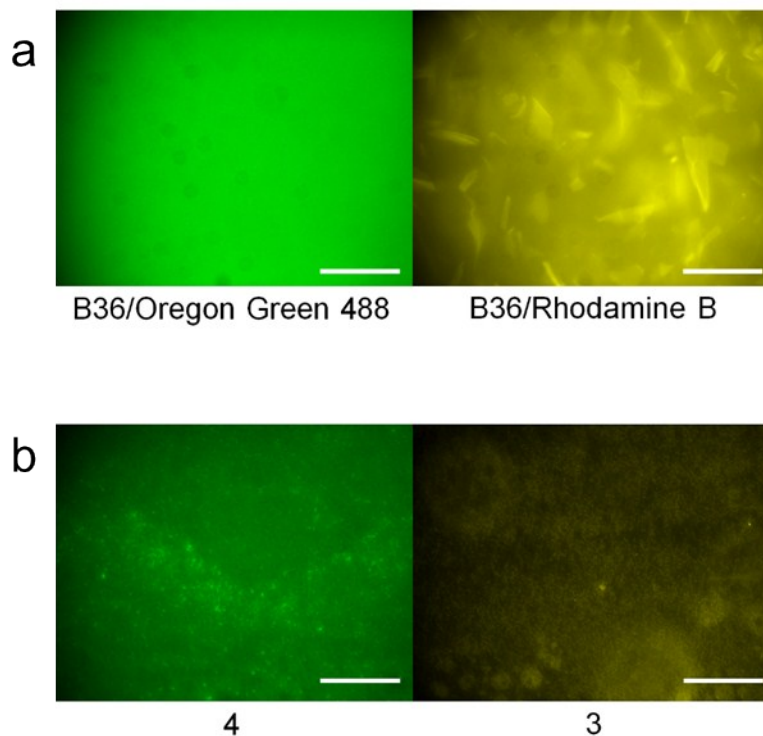


Figure S1. Fluorescent microscopic images of (a) assembly of B36 with unconjugated Oregon Green 488 and unconjugated Rhodamine B, (b) dye-conjugated lipids after compression cycles without B36 (1, 2, 3, and 4). Compared to B36/fluorescent lipid (Figure 1a), images of B36/hydrophilic dye show that there is indistinct dye localization with high background. All scale bars represent 100 μm .

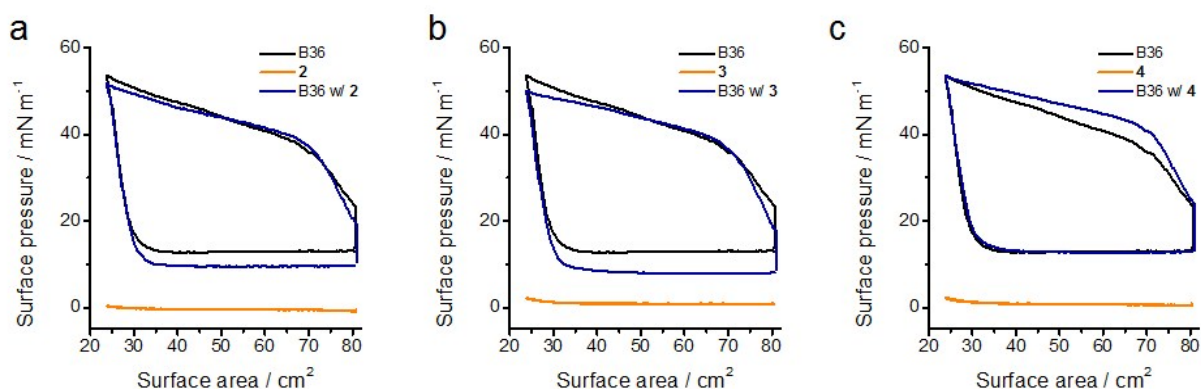


Figure S2. Langmuir isotherms of B36, dye-conjugated lipids (2, 3 and 4), and B36 in the presence of 2, 3 and 4. The curve were obtained by compression/expansion at a rate of $100 \text{ cm}^2 \text{ min}^{-1}$ with a wait time of 450 s between compression and expansion.

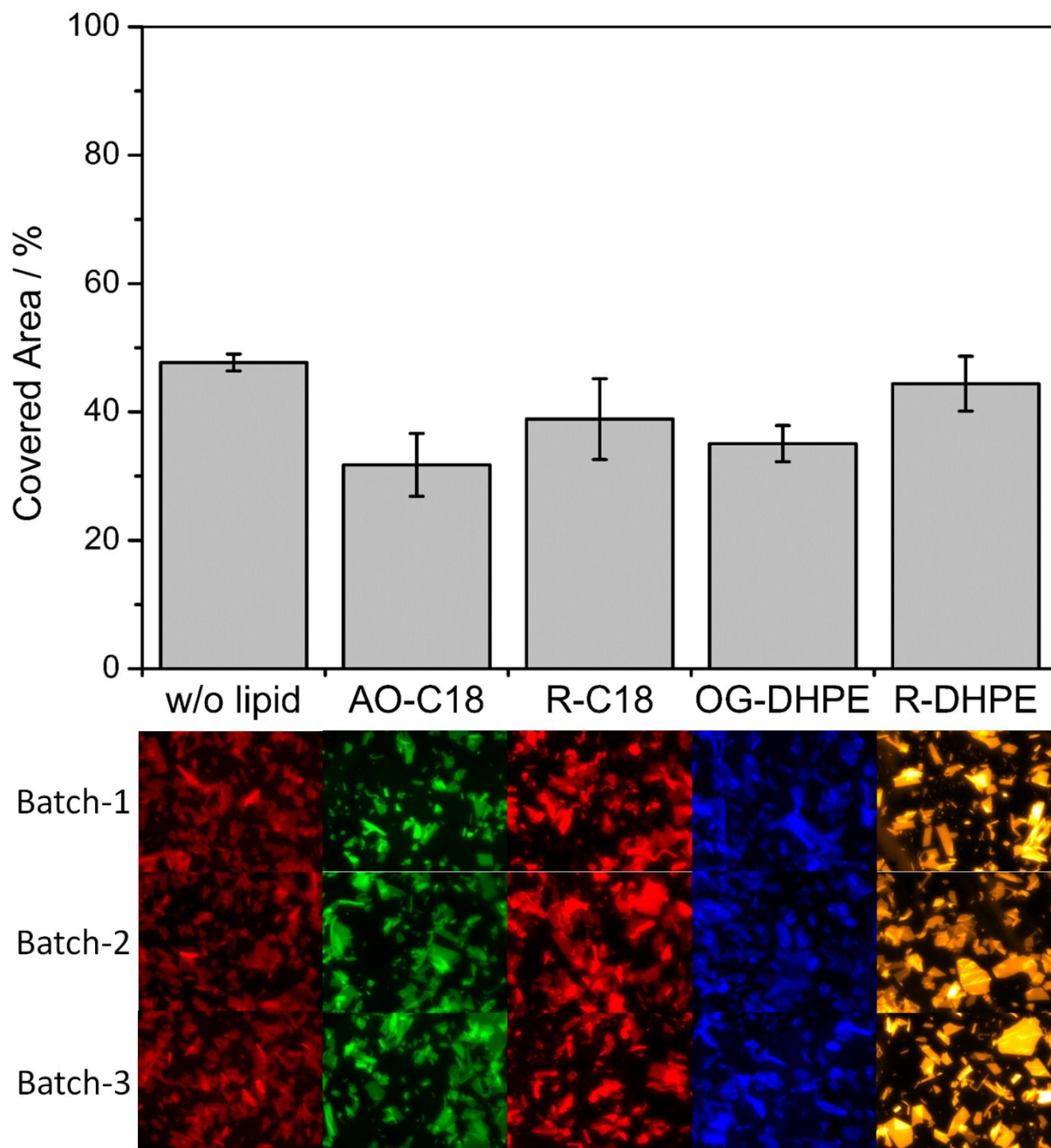


Figure S3. Validation of peptoid nanosheet formation in the presence of **1** – **4**. The sample without lipid was stained with Nile red. The yield of nanosheets were quantified by measurement of the visible area of peptoid nanosheets.⁴ The images were collected by fluorescent microscopy. Nanosheet area was obtained from averaging of three images.

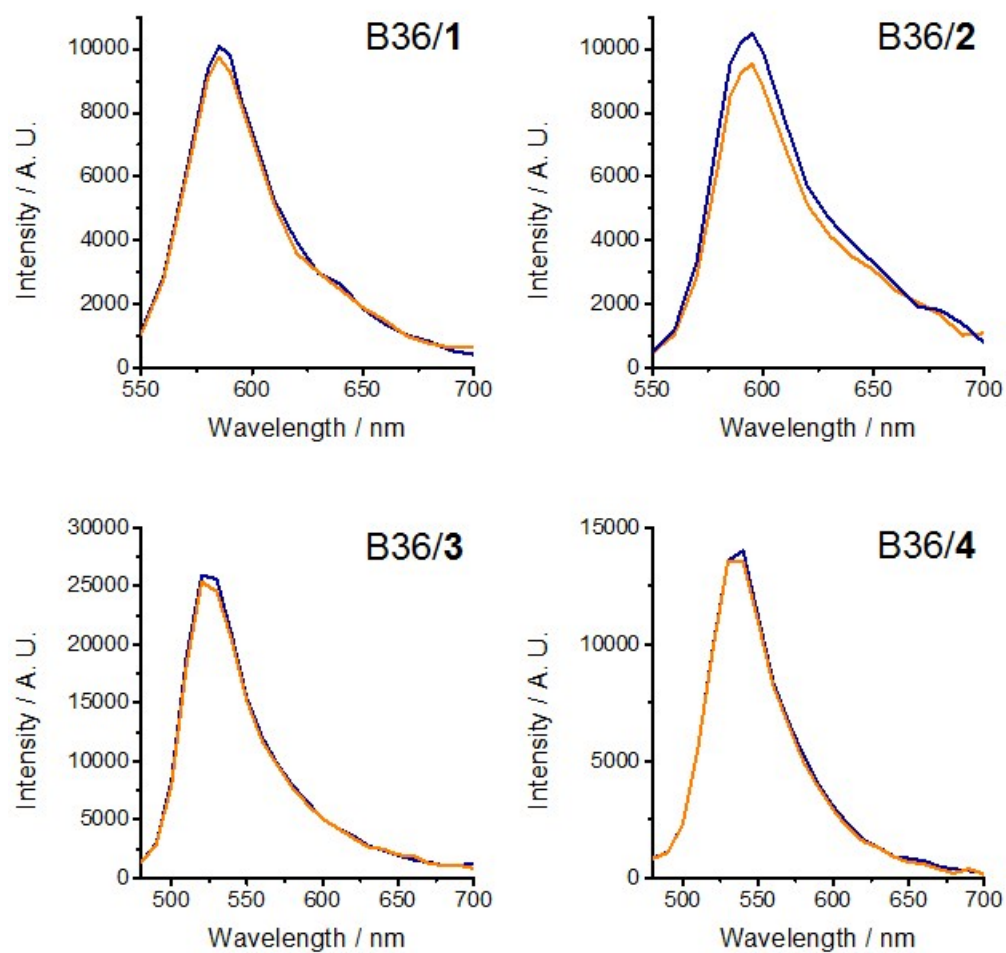


Figure S4. Fluorescence spectra of B36/1, 2, 3, and 4 nanosheets before (blue) and after (orange) dialysis. Fluorescence intensity almost maintained after dialysis, indicating that lipid inserts were stable in peptoid nanosheets.

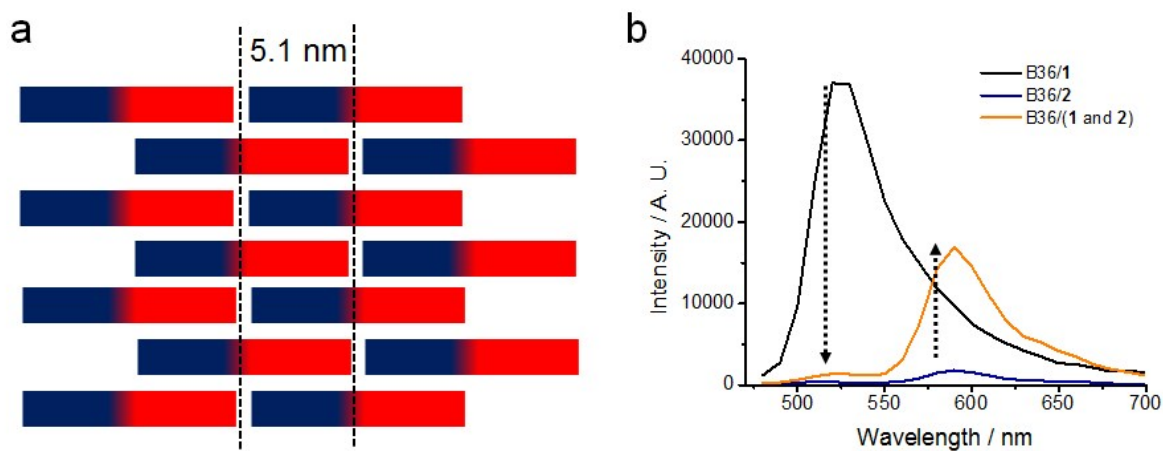


Figure S5. Distance between lipids based on molecular structure and FRET assay. (a) Schematic illustration of brick-like patterned structure of peptoid nanosheets.⁷ The distance between pockets is approximately 5.1 nm. (b) Fluorescence spectra of B36/10 μ M **1**, /10 μ M **2**, and /(10 μ M **1** and 10 μ M **2**) under the excitation wavelength at 450 nm. Using the equation {FRET efficiency = $1 - (\text{Intensity}_{\text{FRET donor/acceptor}} / \text{Intensity}_{\text{FRET donor}})$ } where R_0 is FRET radius, we estimated the lipid-lipid distance to be 4.9 nm. R_0 is 8.4 nm according to the literature. We assumed that all lipids were homogeneously incorporated into peptoid nanosheets and the number of pockets is same with that of peptoid strands.

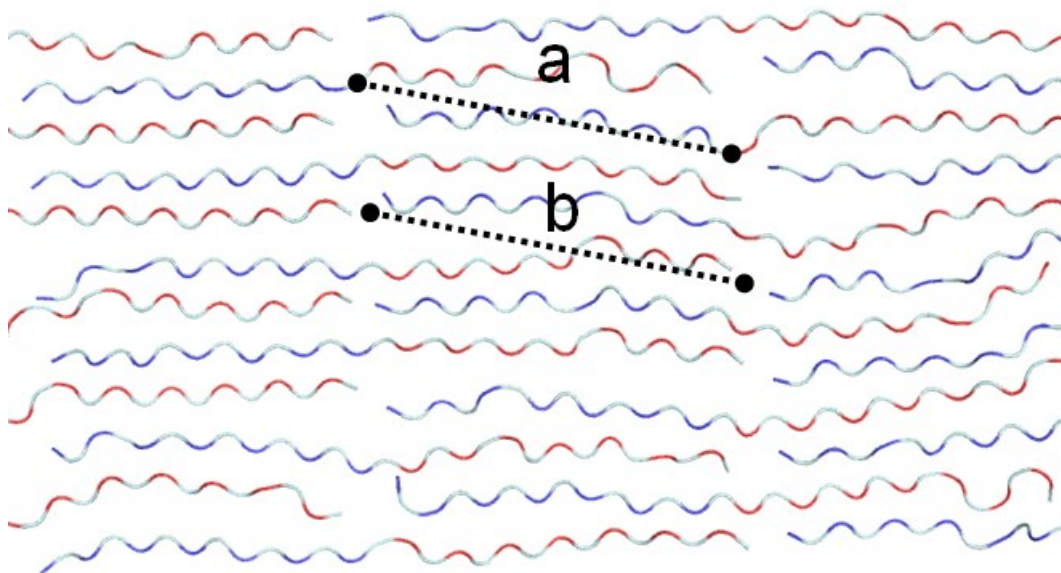
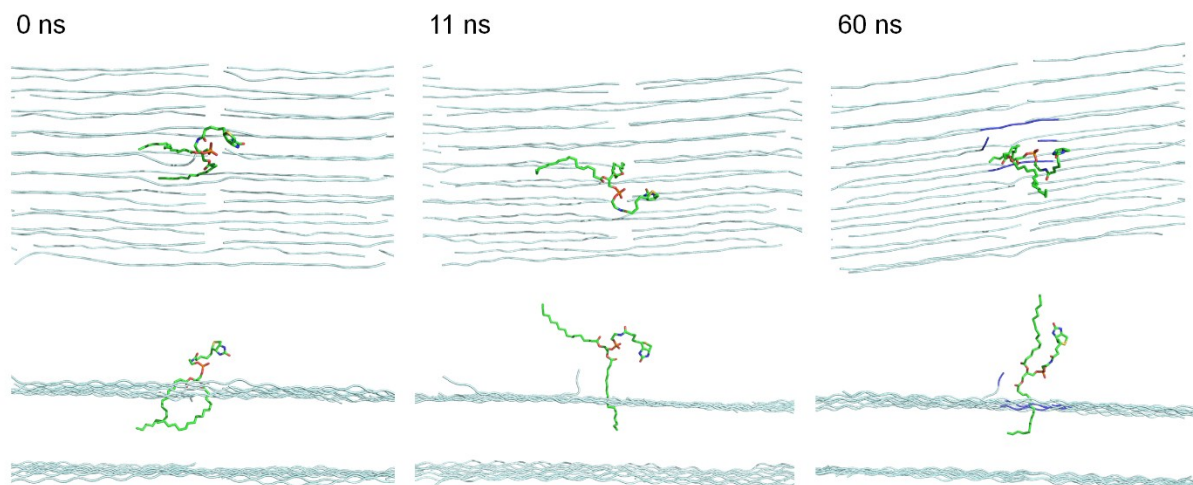


Figure S6. The distance between (a) loops and (b) pockets based on the molecular structure of peptoid nanosheets. Red, blue, and gray represent anionic, cationic, and aromatic residues, respectively.

a



b

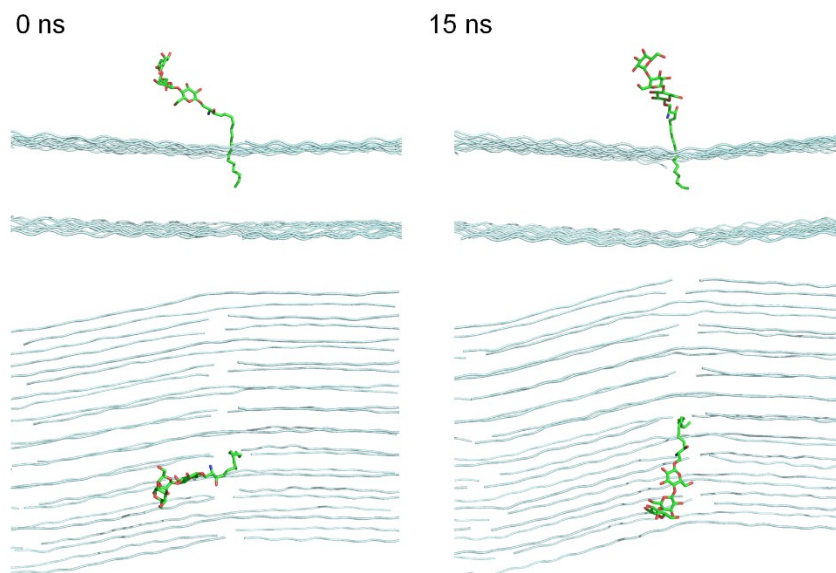


Figure S7. Molecular structure of (a) B36/**5** and (b) B36/**6** by MD simulations. After 11 ns, one of the carbon tails of **5** near the spacing between peptoid strands escaped from peptoid nanosheets. However, another tail in pockets was stable after 60 ns. **6** was also stable in pockets after 15 ns.

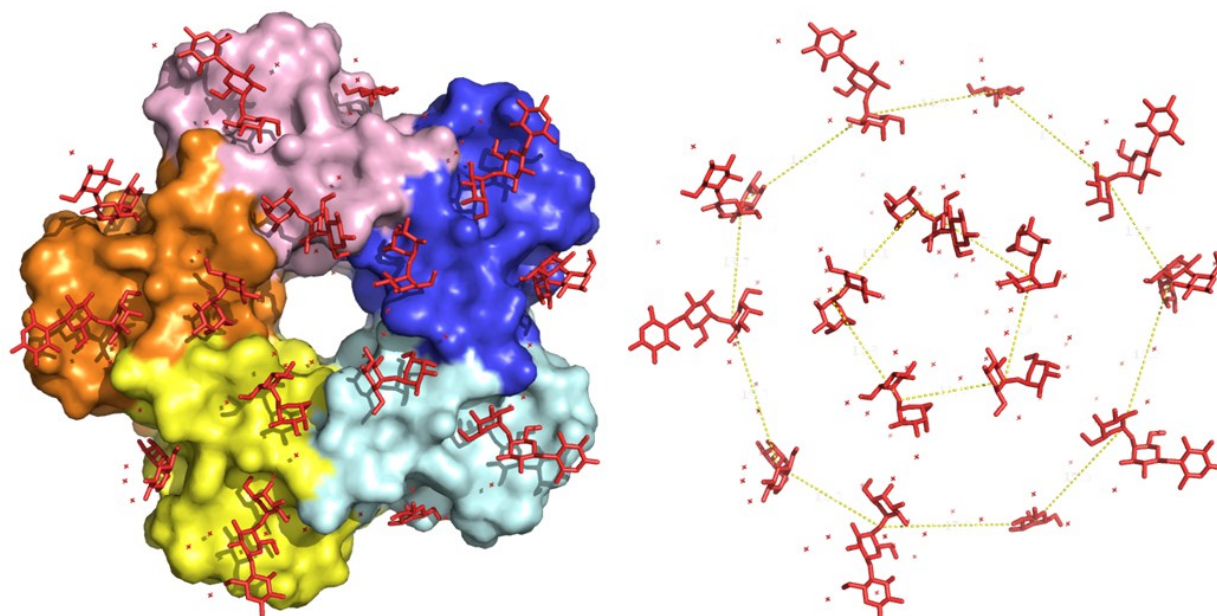


Figure S8. Molecular structure (left) of STX 1B and globotriaose (PDB# 1BOS).⁸ STX 1B is a homopentameric protein and each monomer is depicted by pink, orange, yellow, cyan, and blue. Globotriaose molecules were highlighted by red. The shortest distance between globotriaose molecules is estimated to be 1.4 nm by the average among 15 shortest distances between globotriaose molecules as shown in right image.

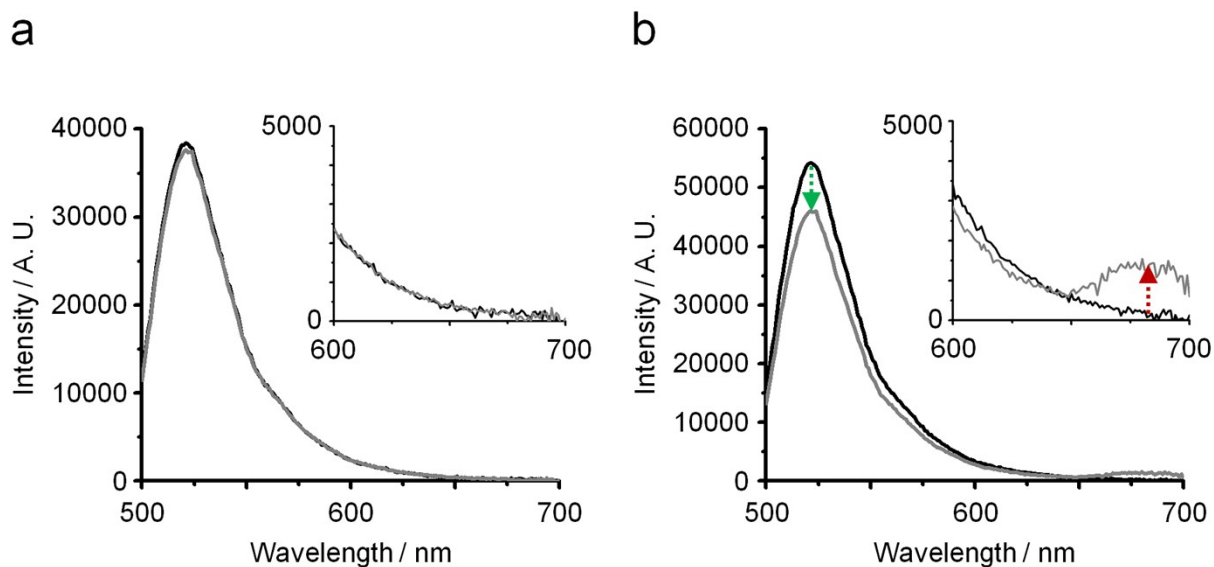


Figure S9. Fluorescence spectra of (a) B36 and (b) B36/6 nanosheets in the absence (black) and presence (gray) of 250 nM STX 1B. Inset is the magnification of fluorescence spectra under the wavelength range from 600 nm to 700 nm. All spectra were obtained under the excitation wavelength at 480 nm.

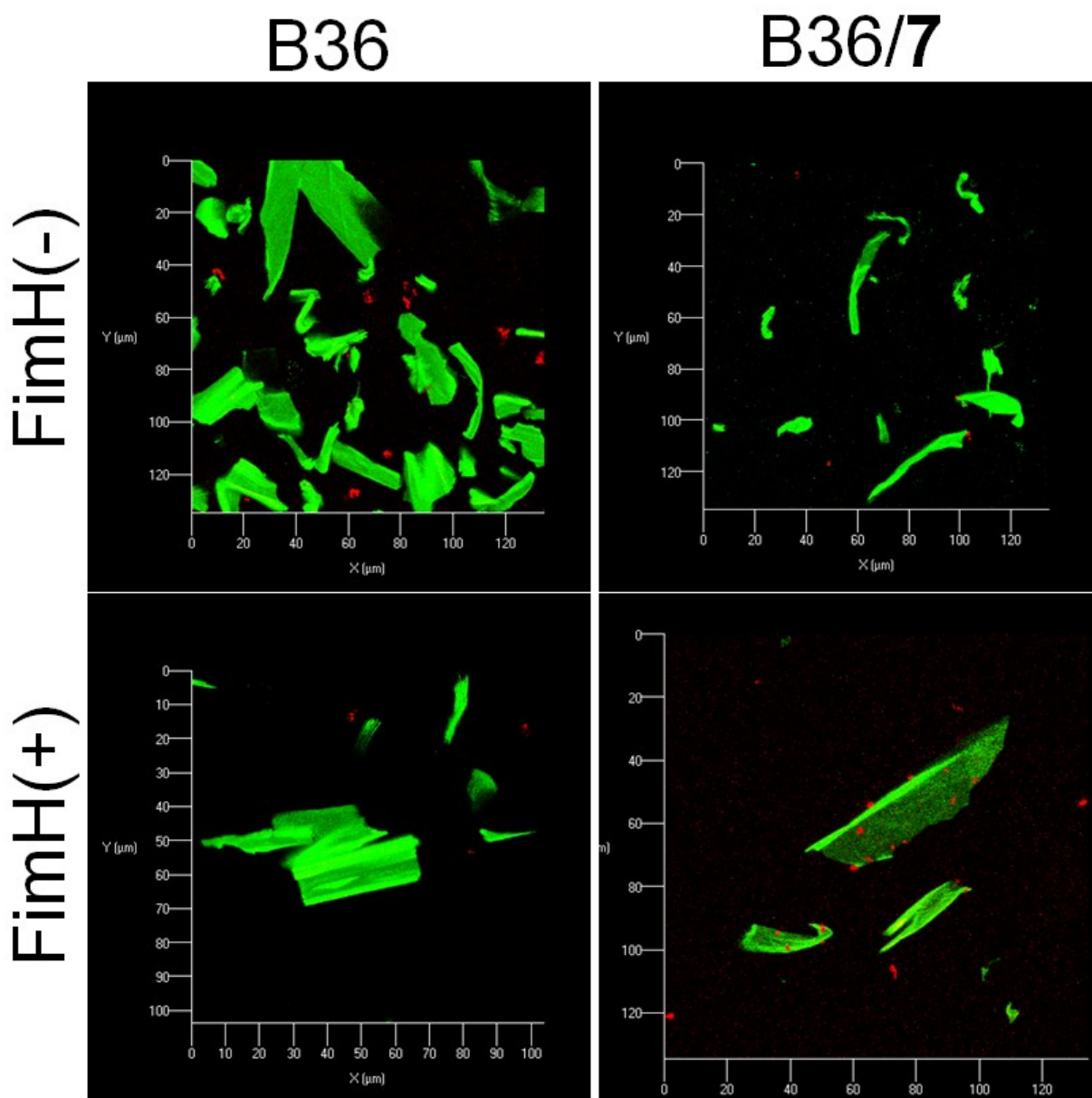


Figure S10. Confocal images of B36, B36/7 in the absence and presence of *E. coli* ORN178 and ORN208. The concentration of **7** is 20 μM. Green is peptoid nanosheets due to Alexa488 conjugation to B36 strands. Red is *E. coli* staining by red-fluorescence proteins.

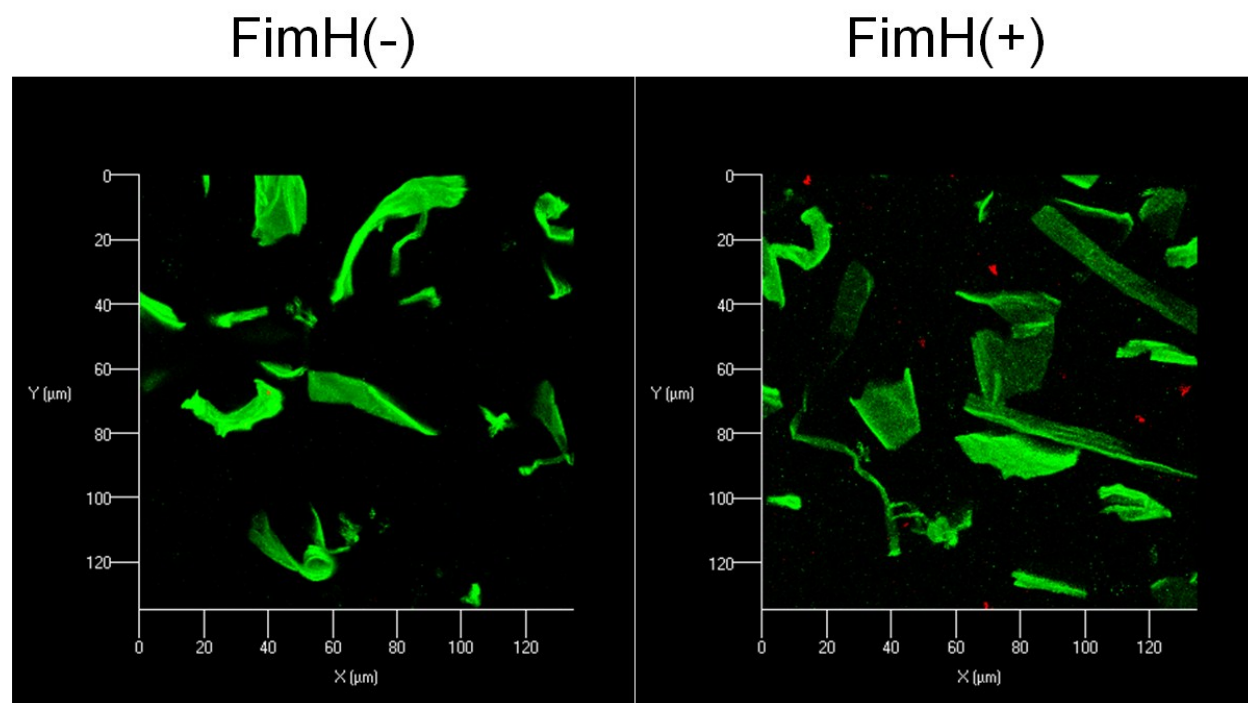


Figure S11. Effect of lipid concentration to capture *E. Coli*. Confocal images of B36/7 in the absence and presence of *E. coli* ORN178 and ORN208. The concentration of 7 is 10 μM . Green is peptoid nanosheets due to Alexa488 conjugation to B36 strands. Red is *E. coli* staining by red-fluorescence proteins.

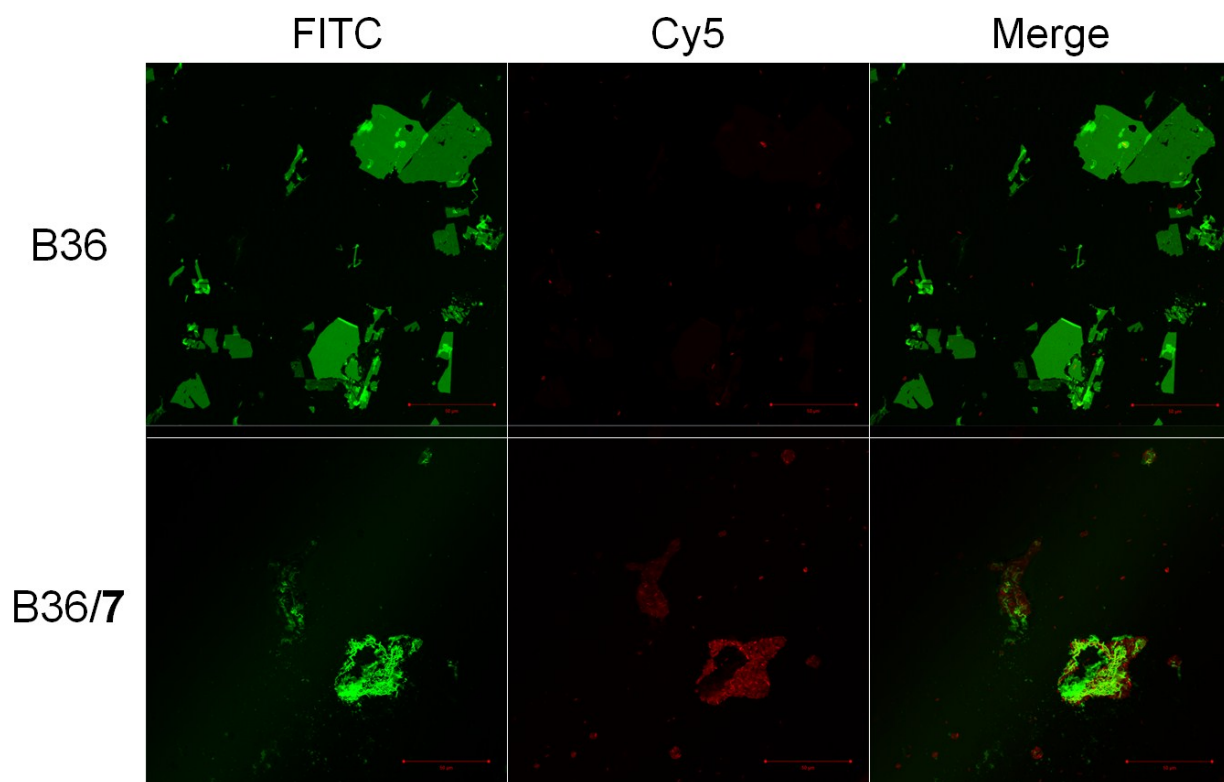


Figure S12. *E. Coli* aggregation on the surface of B36/7. Fluorescent microscopic images of B36 and B36/7 in the presence of *E. coli* ORN178. The concentration of **7** is 20 μ M. Green is peptoid nanosheets due to Alexa488 conjugation to B36 strands. Red is *E. coli* staining by red-fluorescence proteins.

REFERENCES

1. H. Tran, S. L. Gael, M. D. Connolly and R. N. Zuckermann, *J. Vis. Exp.*, 2011, DOI: 10.3791/3373, e3373.
2. S. L. Harris, P. A. Spears, E. A. Havell, T. S. Hamrick, J. R. Horton and P. E. Orndorff, *J. Bacteriol.*, 2001, **183**, 4099-4102.
3. O. O. Abudayyeh, J. S. Gootenberg, S. Konermann, J. Joung, I. M. Slaymaker, D. B. Cox, S. Shmakov, K. S. Makarova, E. Semenova, L. Minakhin, K. Severinov, A. Regev, E. S. Lander, E. V. Koonin and F. Zhang, *Science*, 2016, **353**, aaf5573.
4. B. Sanii, R. Kudirka, A. Cho, N. Venkateswaran, G. K. Olivier, A. M. Olson, H. Tran, R. M. Harada, L. Tan and R. N. Zuckermann, *J. Am. Chem. Soc.*, 2011, **133**, 20808-20815.
5. G. K. Olivier, A. Cho, B. Sanii, M. D. Connolly, H. Tran and R. N. Zuckermann, *ACS Nano*, 2013, **7**, 9276-9286.
6. Y. Guo, C. Sakonsinsiri, I. Nehlmeier, M. A. Fascione, H. Zhang, W. Wang, S. Pohlmann, W. B. Turnbull and D. Zhou, *Angew. Chem. Int. Ed.*, 2016, **55**, 4738-4742.
7. R. V. Mannige, T. K. Haxton, C. Proulx, E. J. Robertson, A. Battigelli, G. L. Butterfoss, R. N. Zuckermann and S. Whitelam, *Nature*, 2015, **526**, 415-420.
8. H. Ling, A. Boodhoo, B. Hazes, M. D. Cummings, G. D. Armstrong, J. L. Brunton and R. J. Read, *Biochem.*, 1998, **37**, 1777-1788.